Pressure-Induced Valence and Structural Changes in YbMn$_2$Ge$_2$—Inelastic X-ray Spectroscopy and Theoretical Investigations

Ravhi S. Kumar,[†,*] A. Svane,[‡] G. Vaitheeswaran,[§] Y. Zhang,[†] V. Kanchana,[∥] M. Hofmann,[⊥] S. J. Campbell,[#] Yuming Xiao,[▽] P. Chow,[▽] Changfeng Chen,[†] Yusheng Zhao,[†] and Andrew L. Cornelius[†]

[†]Department of Physics and Astronomy and HiPSEC, University of Nevada Las Vegas, Las Vegas, Nevada 89154, United States

[‡]Department of Physics and Astronomy, Aarhus University, DK-8000 Aarhus C, Denmark

[§]Advanced Centre of Research in High Energy Materials (ACRHEM), University of Hyderabad, Hyderabad -500 046, Andhra Pradesh, India

[∥]Department of Physics, Indian Institute of Technology Hyderabad, Ordnance Factory Estate, Yeddumailaram − 502205, Andhra Pradesh, India

[⊥]Technische Universität München, FRM-II, 85748, Garching, Germany,

[#]School of Physical, Environmental and Mathematical Sciences, The University of New South Wales Australian Defense Force Academy, Canberra, ACT 2600, Australia

[▽]HPCAT, Carnegie Institution of Washington, Argonne National Laboratory, Argonne, Illinois 60439, United States

ABSTRACT: The pressure-induced valence change of Yb in YbMn$_2$Ge$_2$ has been studied by high pressure inelastic X-ray emission and absorption spectroscopy in the partial fluorescence yield mode up to 30 GPa. The crystal structure of YbMn$_2$Ge$_2$ has been investigated by high pressure powder X-ray diffraction experiments up to 40 GPa. The experimental investigations have been complemented by first principles density functional theoretical calculations using the generalized gradient approximation with an evolutionary algorithm for structural determination. The Yb valence and magnetic structures have been calculated using the self-interaction corrected local spin density approximation. The X-ray emission results indicate a sharp increase of Yb valence from $v = 2.42(2)$ to $v = 2.75(3)$ around 1.35 GPa, and Yb reaches a near trivalent state ($v = 2.95(3)$) around 30 GPa. Further, a new monoclinic $P1$ type high pressure phase is found above 35 GPa; this structure is characterized by the Mn layer of the ambient ($I4/mmm$) structure transforming into a double layer. The theoretical calculations yield an effective valence of $v = 2.48$ at ambient pressure in agreement with experiment, although the pure trivalent state is attained theoretically at significantly higher pressures (above 40 GPa).
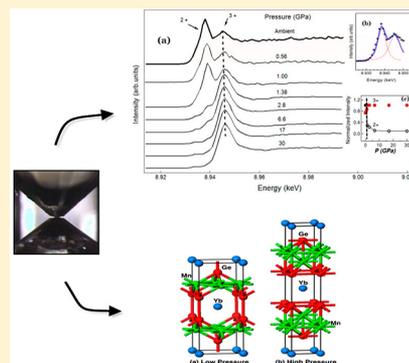
1. INTRODUCTION

Solids containing elements from the rare earth series show interesting and unusual behavior associated with the versatility of the manifold of *4f* electrons, including heavy fermion and intermediate valence behavior, superconductivity, and Kondo screening.[1−4] In Yb compounds the Yb ions may be found either in the $4f^{13}$ (3+) or the $4f^{14}$ (2+) configuration. The energy difference between these two valence states is in many cases small, and therefore rapid configurational changes can be induced by small changes in temperature, pressure, or magnetic field.[5] In this paper we explore the effect of high pressure on the intermediate valence compound YbMn$_2$Ge$_2$ together with complementary theoretical studies.

YbMn$_2$Ge$_2$ belongs to the rich class of rare earth intermetallic compounds of the form RT$_2$X$_2$, where R = rare earth, T = transition metal, and X = Si or Ge. They form mainly in the body-centered tetragonal ThCr$_2$Si$_2$ structure,[6] with a variety of

magnetic structures due to the intricate interactions between the magnetic moments of the R and T ions.[7] In addition, R = Ce, Eu, or Yb compounds can possibly display a fluctuating valence. They have been studied intensely, because of the unconventional superconductivity exhibited in some of these materials, and their low-temperature properties are influenced by the presence of an unconventional quantum critical point. Yb is found in an intermediate valence state in YbMn$_2$Ge$_2$ at ambient conditions, as determined from the anomalously large lattice constant,[8] ^{170}Yb Mössbauer spectrum,[9] and core-level photoemission spectrum.[10] The lattice constant anomaly leads to an estimate of the effective Yb valence $v = 2.35$,[8] while according to both the Mössbauer[9] and photoemission[10] experiments the effective valence is close to $v = 2$. The valence

changes with alloying,[9,11] temperature,[11] and hydrostatic pressure.[12,13] In the $YbMn_2Si_{2-x}Ge_x$ alloys, traces of divalency appear for $x > 1.2$ in the Mössbauer spectra,[9] while neutron diffraction experiments[11] suggest a valence transition around $x = 1.6$. Pressure experiments on $YbMn_2Ge_2$ show an anomalously large volume contraction up to an applied pressure of 1.5 GPa, reminiscent of similar transitions in the ytterbium chalcogenides.[14−16] The pressure−volume relation above this pressure is similar to that of $YbMn_2Si_2$,[12] suggesting that $YbMn_2Ge_2$ is in a trivalent state above 1.5 GPa.

Like many compounds in the RMn_2X_2 series (X = Si, Ge), the magnetic structure of $YbMn_2Ge_2$ is complex[11,12,17−19] and dominated by the exchange interaction of the Mn moments. The system is paramagnetic above T_{N1} = 510 K with Mn moments ordering antiferromagnetically and collinearly in the basal plane at T_{N1} to form the AFl structure in the interval $T_{N1} > T > T_{N2}$ =185 K.[17] Below T_{N2}, the Mn moments form the canted noncollinear antiferromagnetic structure[17] AFmc (the magnetic structures are described using the notation of Venturini et al. in ref 18, where the AFl and AFmc structures are depicted). The magnetic order of $YbMn_2Ge_2$ is also found to change with the rapid Yb valence change that occurs with pressure at room temperature around 1.5 GPa.[12,18] Above 1.5 GPa the Mn moments order ferromagnetically within planes perpendicular to the c-axis, with an antiferromagnetic stacking of adjacent Mn planes[12] (AFil structure as in ref 18). The similarity between the magnetic structure of $YbMn_2Ge_2$ above $p \sim 1.5$ GPa and the high temperature magnetic structure of $YbMn_2Si_2$ is consistent with the proposition that the Yb valence is similar in these two cases, that is, close to trivalency. Temperature dependent resistivity measurements show that the occurrence of two magnetic transition temperatures prevail at high pressure.[19,20]

In the present work, the pressure induced changes in the electronic structure of $YbMn_2Ge_2$ at room temperature have been studied using high pressure X-ray diffraction (HPXRD), resonant X-ray emission spectroscopy (RXES), and X-ray absorption spectroscopy (XAS) in the partial fluorescence yield (PFY) mode for pressures from ambient to 40 GPa, supported by theoretical calculations. The HPXRD measurements revealed a structural phase transformation around 34 GPa. Recently RXES has been applied to investigate a variety of Yb intermetallic and other heavy fermion compounds.[21−23] RXES enables the valence to be determined with incident photon energies being selected to enhance signals from different valence states. Theoretical calculations have been carried out for $YbMn_2Ge_2$ using the self-interaction corrected local spin-density (SIC-LSD) method. This ab initio electronic structure method allows us to study the pure divalent and trivalent states of Yb and also to approximate the intermediate valence state using the total energy to determine the ground state. This method has previously been applied for determining the Yb valence in intermetallic compounds.[5,24] Furthermore, calculations using the generalized gradient approximation (GGA) and an evolutionary algorithm have been performed to investigate the structural transition at high pressure.

2. EXPERIMENTAL SECTION

The polycrystalline sample of $YbMn_2Ge_2$ was prepared and characterized elsewhere[13] with powder X-ray diffraction confirming the single phase nature of the sample. The HPXRD experiments were carried out up to 40 GPa at Sector 16 ID-B of the Advanced Photon Source in the angle dispersive geometry. The sample with a few ruby grains was introduced into a 135 μm hole of rhenium gasket preindented to 50 μm with a 4:1 methanol−ethanol pressure medium and pressurized using a Mao-Bell type diamond anvil cell. The pressure in the diamond cell was determined using the ruby fluorescence technique. Diffraction images were collected using a MAR-345 imaging plate with an incident wavelength of λ = 0.344682 Å and integrated using Fit2D software.[25] The spectra were further analyzed using the Rietveld (RIETICA) package.[26]

The X-ray emission data were collected at Sector 16 ID-D of the Advanced Photon Source by focusing the incident X-ray beam to dimensions of 20 μm × 50 μm. The PFY and RXES experiments were performed at the Yb L_3 absorption edge (8.944 keV) with an energy resolution of 1 eV.

3. THEORETICAL ANALYSES

The theoretical description of fluctuating valence systems is notoriously difficult.[27] In the present work the electronic structure of $YbMn_2Ge_2$ has been calculated with SIC-LSD,[28−30] where the effective one-electron potential includes a correction for the spurious interaction of individual electrons with themselves.[28] This term favors the formation of spatially localized states as compared to extended Bloch waves and leads to a scheme for the calculation of cohesive properties of rare-earth compounds.[31,32]

In Yb compounds[5,24] the SIC-LSD method may describe the pure trivalent and divalent configurations of Yb as well as providing an approximate ansatz for the intermediate valence state. The computed total energy for each of these three cases determines the ground state configuration. The divalent state is realized by applying the self-interaction correction to all 14 f-electrons of Yb, while the pure trivalent state is realized by applying the self-interaction to 13 f electrons and prohibiting the 14th f electron from being occupied by projecting it out of the band subspace. In the approximate model of the intermediate valence state, 13 f electrons are localized on each Yb ion by the self-interaction correction, while the 14th f electron is allowed to hybridize and form a band that is pinned at the Fermi level. The degree of filling of this band determines the effective Yb valence. If the filling is x, it implies that the wave function may be decomposed into a Yb f^{14} component with weight x and a Yb f^{13} component with weight $1 − x$. Hence, this band filling is directly comparable to the effective valence as derived from an experimental spectrum, which involves a superposition of components from either of the two Yb configurations, f^{13} and f^{14}, as is the case for the partial fluorescence yield and resonant X-ray emission spectroscopy experiments. The method has previously been applied to $YbAl_3$ under pressure[23] and to the pressure induced isostructural transitions in the Yb chalcogenides.[33] The present implementation of the SIC-LCD method includes spin−orbit coupling and uses the linear muffin-tin orbital method[34] in the tight-binding formulation,[35] with technical details described in ref 27.

To search for the stable and most competitive metastable structures of $YbMn_2Ge_2$ at high pressures the USPEX evolutionary algorithm code[36] has been applied. This method has been widely used in high pressure structure predictions. The predicted structures are fully relaxed using the spin-polarized density functional theory and the GGA[37] for the exchange-correlation functional as implemented in the VASP package.[38] The structure predictions are based on calculations using unit cells containing two formula units of $YbMn_2Ge_2$ (10 atoms). No preimposed symmetry constraint or experimental information is used in these calculations. At least 20 nonequivalent k points are used for the Brillouin-zone sampling
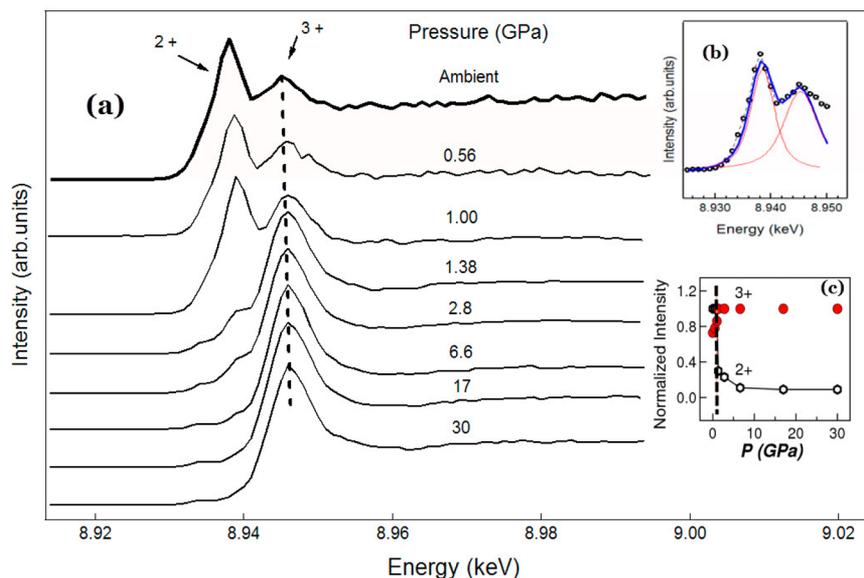
Figure 1. (a) X-ray absorption spectra collected in the PFY mode at various pressures. The arrows indicate the contributions from the Yb^{2+} and Yb^{3+} components. (b) Fitting of the divalent and trivalent peak profiles in the ambient spectrum is shown. The circles represent the experimental data, and the solid lines are the fittings. (c) The intensity corresponding to the divalent component decreases rapidly around 1.4 GPa (marked by the vertical line) as the pressure increases, while the intensity of the trivalent component increases.

during the structure search, resulting in a total energy convergence of less than 2 meV/atom. We employed the standard setting parameters for the structure search. The first generation of structures is generated randomly, and the number of structures in each generation is 30. The most favorable 65% of structures in each generation are chosen to predict the next generation by heredity (60%), mutation (20%), and permutation (20%). In the enthalpy calculations, an energy cutoff of 400 eV and an $8 \times 8 \times 4$ k-point mesh were used to obtain reasonable convergence on total energy ($<10^{-6}$ eV) and stress ($<10^{-4}$ eV/Å). The lattice parameters calculated for $YbMn_2Ge_2$ ($I4/mmm$ structure) under ambient conditions are $a = 3.969$ Å and $c = 10.931$ Å. The deviations of these calculated values from the present experimental values of $a = 4.0432$ Å and $c = 10.948$ Å are likely to reflect the treatment of the Yb f-electrons as itinerant states within these calculations.

4. RESULTS AND DISCUSSION

4.1. Pressure Induced Valence Change. The X-ray absorption spectra collected in the partial fluorescence yield mode at pressures up to 30 GPa are shown in Figure 1. The PFY spectrum of $YbMn_2Ge_2$ at ambient pressure shows a two peak structure with a 2+ component ($E_{in,2+} = 8.938$ keV) and a 3+ component ($E_{in,3+} = 8.945$ keV). The higher intensity observed for the first peak indicates that Yb is predominantly in the divalent state, consistent with the results of the neutron diffraction,[8] Mössbauer,[9] and photoemission[10] experiments. As shown by the inset to Figure 1, the intensities of the 2+ and 3+ components change as pressure increases, with the intensity of the 3+ peak found to dominate above a transition pressure of 1.38 GPa. The reduction in the intensity of the 2+ peak indicates a change in the Yb valence toward the trivalent state. The intensity of the 2+ peak vanishes above ∼20 GPa, indicating that Yb is essentially in a trivalent state above this pressure.

The RXES spectra were collected by varying the incident energy across the L3 edge of Yb. When the incident energy

approaches the absorption threshold of Yb^{2+} and Yb^{3+}, the intensity corresponding to the 2+ and 3+ features observed in the emission spectra are resonantly enhanced. The spectra collected (Figure 2) above and below the transition pressure
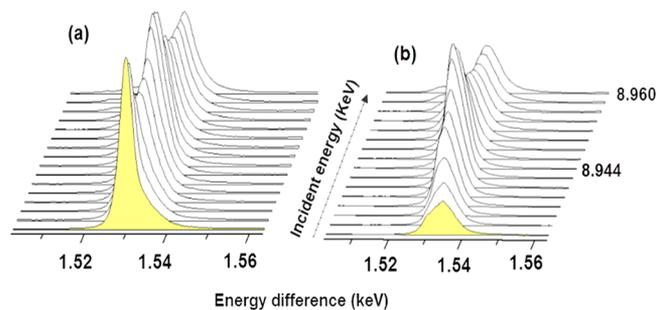
Figure 2. Series of RXES spectra collected below and above the transition pressure of 1.4 GPa for a range of incident energies. (a, b) RXES spectra at $p = 1$ and 6.8 GPa, respectively. The X-ray emission intensities are shown as a function of the transferred energy, and the incident energy is shown on the third axis.

(∼1.38 GPa) are found to be consistent with the PFY measurements. The average values of the Yb valence for $YbMn_2Ge_2$ under pressure were estimated from the PFY spectra of Figure 1 by substituting the integrated intensities of the 2+ and 3+ components at each pressure into the linear expression $v = 2 + I(3+)/[I(2+) + I(3+)]$, where $I(2+)$ and $I(3+)$ represent the 2+ and 3+ intensities, respectively.[21−23] Fitting of the 2+ and 3+ peaks was done by adjusting the relative weights of the two line shapes using a Voigt type function. For the best fit, we have obtained the full width at half-maximum (fwhm) of 5 and 6 eV for the divalent and trivalent components, respectively. The small pre-edge features appearing around 8.934 keV above 1.38 GPa are attributed to the 3d−2p quadrupole transitions and are not taken into account for the fit. The branching of the 2+ and 3+ components in the RXES spectra (Figure 2) show clear

changes in the intensity ratios at 1.4 GPa similar to the PFY experiments.

The RXES spectral cross section is described by the Kramers-Heisenberg equation

$$F(\Omega, \omega) = \sum_f \left| \sum_i \frac{\langle f|T^*|n\rangle\langle n|T|g\rangle}{E_g - E_i + \Omega - i\Gamma_{2p}} \right|^2 \times \frac{\gamma/\pi}{(E_g - E_f + \Omega - \omega)^2 + (\gamma)^2} \tag{1}$$

where $|n\rangle$ represents the intermediate state, $|g\rangle$ represents the ground state, and $|f\rangle$ the final state, respectively. E_g and E_f are the ground state and final state energies. The incident and emitted energies are indicated by Ω and ω. T is the optical transition operator. Energy conservation in the RXES process is conserved within the energy widths Γ_{2p} and γ in the equation. The RXES process is unique since it is bulk sensitive and not surface dependent like other excitation spectroscopic techniques such as XAS. RXES provides complementary information obtained from XAS as well as details regarding electron configuration and hybridization. However, decomposition of line shapes of different valence states in the RXES spectra is difficult due to underlying fluorescence signals. The fitting and analysis were carried out using the procedure outlined in refs 22. and 23.

The resultant values of the average Yb valence are plotted as a function of pressure in Figure 3.
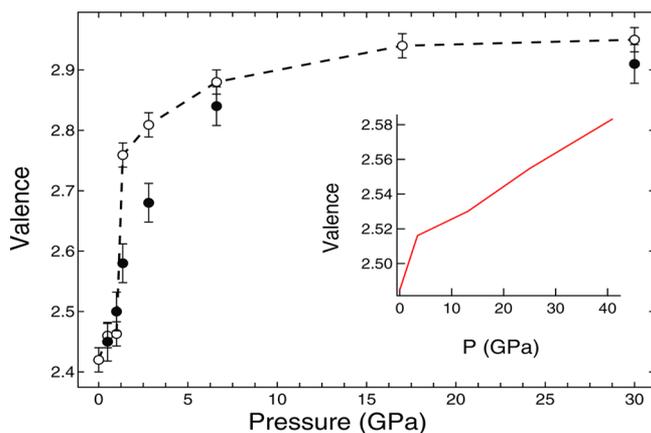
Figure 3. Average Yb valence as a function of pressure for YbMn₂Ge₂ up to 30 GPa. The filled circles represent the values derived from RXES experiments, while the open circles are from PFY experiments. The inset shows the theoretical values determined for pressures up to 40 GPa as described in the text.

The discrepancy in the valence between PFY and RXES measurements is due to the ambiguity in the estimation of intensity due to fluorescence peak arising between 2+ and 3+ components in the resonant emission.

As shown in Figure 3, the average Yb valence increases from $\nu = 2.42(2)$ at ambient pressure to $\nu = 2.78(3)$ at 1.4 GPa at a rate of $d\nu/dp \sim 0.27$ GPa^{-1}. From 2–10 GPa the valence increases at a slower rate ($d\nu/dp \sim 0.015$ GPa^{-1}), reaching $\nu = 2.91(4)$. Above 10 GPa the spectra remain relatively unchanged, and the average valence approaches a saturation value of $\nu = 2.95(4)$ with no further increase in the valence observed above 25 GPa. The calculations find the intermediate valence state as the ground state through the entire pressure

range, with a valence increase at a rate $d\nu/dp \sim 0.005$ GPa^{-1}, that is, significantly slower than observed (inset to Figure 3).

The significant change in average valence observed around 1.4 GPa is in excellent agreement with the high pressure neutron diffraction experiments,[12,13] which observe a 7% collapse in the specific volume between 1.0 and 1.5 GPa. Similar volume collapses occur for the Yb chalcogenides[14–16] and indicate a change in 4f occupancy. However, no structural transition is associated with the transition, despite the change in magnetic ordering at this pressure.[12] Compared to other Yb systems, such as YbAl₂ and YbAl₃ and the monochalcogenides, which are all characterized by sluggish transitions,[14–16,21–23] the pressure induced valence transition in YbMn₂Ge₂ around 1.4 GPa appears more abrupt.

4.2. Phase Transition at High Pressure. The evolution of the structural changes in YbMn₂Ge₂ with applied pressure in the range 0–40 GPa is shown by the set of X-ray diffraction patterns in Figure 4. YbMn₂Ge₂ crystallizes in the layered
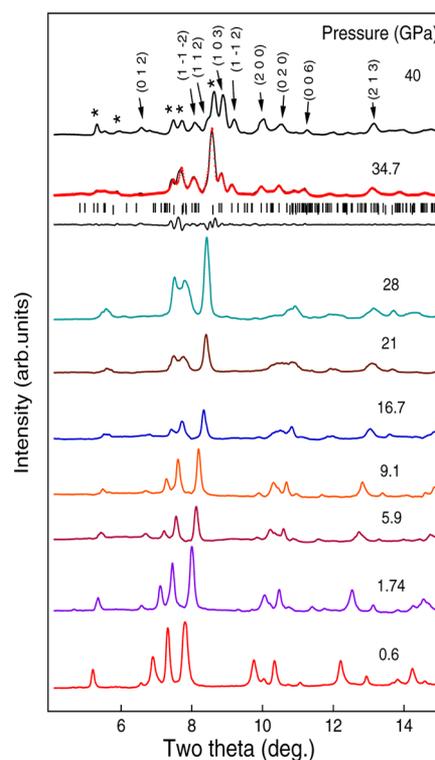
Figure 4. High pressure X-ray diffraction patterns at various pressures up to 40 GPa (incident wavelength $\lambda = 0.344682$ Å). The evolution of the high pressure $P1$ type monoclinic phase is observed around 35 GPa.

ThCr₂Si₂-type body centered tetragonal structure with space group $I4/mmm$ (No. 139). At ambient conditions we obtained lattice parameters $a = 4.0432(1)$ Å and $c = 10.940(8)$ Å, in excellent agreement with earlier reports.[8,12,17] The diffraction patterns showed no changes in the low pressure region—especially around 2 GPa, which is consistent with the neutron experiments[12]—and the diffraction peaks can be indexed with the tetragonal structure up to 21 GPa. Around 28 GPa a splitting in the diffraction peaks located around $2\theta = 7.6°$ is observed with further new diffraction lines also observed around $2\theta = 7.6°$.

Even though the tetragonal peaks remain at pressures above 28 GPa, the splitting and the observation of new diffraction

Table 1. Structural Parameters of YbMn$_2$Ge$_2$[a]

	low pressure phase		high pressure phase	
	pressure = 0 GPa		pressure = 35 GPa	
	space group $I4/mmm$ (No. 139)		space group $P1$ (No. 1)	
	theory	experiment	theory	experiment
cell parameters	a = 3.969 Å	a = 4.0516(1) Å	a = 3.986 Å	a = 3.8458(3) Å
			b = 3.989 Å	b = 3.9701(3) Å
	c = 10.931 Å	c = 10.854(6) Å	c = 8.265 Å	c = 8.308(1) Å
			α = 89.99°	α = 89.81(6)°
			β = 76.05°	β = 79.32(9)°
			γ = 89.99°	γ = 91.31(1)°
	Yb (0,0,0)	Yb (0,0,0)	Yb1 (0.6160, 0.2928, 0.8129)	
	Ge (0,0,0.3777)	Ge (0,0, 0.3924)	Yb2 (0.1160, 0.7928, 0.8129)	
	Mn (0,0.5,0.25)	Mn (0,0.5,0.25)	Ge1 (0.2411, 0.2929, 0.5627)	
			Ge2 (0.9909, 0.2929, 0.0631)	
			Ge3 (0.7412, 0.7929, 0.5627)	
			Ge4 (0.4909, 0.7929, 0.5627)	
			Mn1 (0.8247, 0.2930, 0.3952)	
			Mn2 (0.9074, 0.7930, 0.2306)	
			Mn3 (0.4074, 0.2930, 0.3952)	
			Mn4 (0.3247, 0.7929, 0.3952)	
V_0 (Å^3)/f.u	83.9[b]	89.1[d]		
	86.1[c]			
B_0 (GPa)	114[b]	86[d]		
B_0'	6.1[b]	6[d]		
μ(Mn) (μ_B)	2.09[b]	2.5[e]		
ν (Yb)	2.48[b]	2.42[d]		
P_{val} (GPa)	42[b]	1.4[f]		
P_{mag} (GPa)	1.2[b]	1.25[g]		
P_{struc} (GPa)	30[c]	35[d]		
E (AFil) (meV)	8[b]			
E (F) (meV)	39[b]			

[a]At ambient conditions Yb is at 2a, Ge is at 4d, and Mn is at 4e positions of the $I4/mmm$ structure. V_0 is the equilibrium volume per formula unit, B_0 is the bulk modulus, and B_0' is its pressure derivative. M (Mn) is the Mn magnetic moment and ν (Yb) the effective valence of Yb ions. P_{val} is the pressure for the Yb valence transition, while p_{mag} and p_{struc} denote the magnetic and structural transition pressures. E(AFil) and E(F) are the total energy of the states with AFil and ferromagnetic arrangement of Mn moments, respectively, given in meV per formula unit and relative to the AFl ground state.[20] [b]Present work (as calculated using the SIC-LSD technique; section 2.2). [c]Present work (as calculated using the GGA technique; section 2.2). [d]Present work, except where noted. For pressures above 2 GPa. [e]Ref 17. [f]Onset, transition completed around 20 GPa. [g]Ref 19.

peaks indicate the appearance of a new pressure induced phase. In order to identify the structure at high pressures, we carried out extensive theoretical simulations as a search to match the structure for pressures above 35 GPa, using the USPEX evolutionary algorithm discussed in section 3.

Even though the ambient $I4/mmm$ crystal symmetry remains stable at high pressure, our calculations show that there exists at high pressures a monoclinic ($P1$) structure of YbMn$_2$Ge$_2$ with lower enthalpy. The predicted structural parameters and atomic positions are presented in Table 1. As the experimental diffraction patterns above 28 GPa contained both the monoclinic and tetragonal phases, a Lebail fitting is shown in the table for the mixed phase at 34.7 GPa. The experimental cell parameters are also presented. Figure 5 shows a comparison of the tetragonal $I4/mmm$ structure of YbMn$_2$Ge$_2$ at ambient conditions (Figure 5a) and the monoclinic P1 structure at high pressure (Figure 5b). The structures are in fact similar since the high pressure structure is quite close to tetragonal symmetry. The most distinct change after the pressure induced phase transition is that the single Mn layers of the $I4/mmm$ structure transform into double layers rotated by 45°, leading to a contraction of the unit cell volume. As shown by the enthalpy values calculated for the two structures as functions of pressure
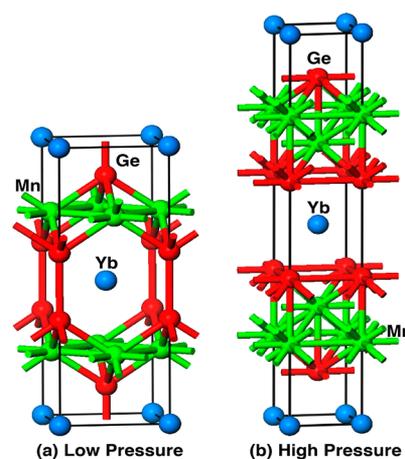
Figure 5. (a) Body-centered tetragonal ($I4/mmm$) structure of YbMn$_2$Ge$_2$ at ambient conditions. (b) Monoclinic ($P1$) structure of YbMn$_2$Ge$_2$ at high pressures (~28 GPa). The unit cell is plotted in tetragonal-like form for more direct comparison with the bct structure.

(Figure 6), a phase transition is expected to occur around 30 GPa. This predicted behavior agrees well with the fact that the
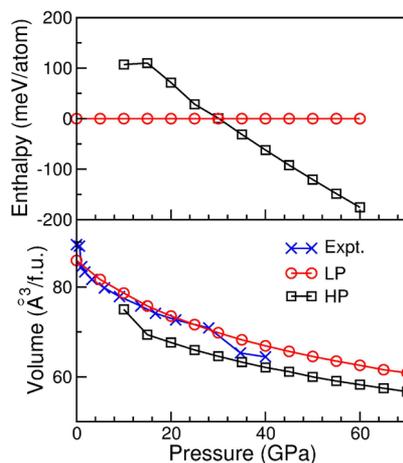
Figure 6. Relative enthalpies of body-centered tetragonal ($I4/mmm$) structure and the monoclinic ($P1$) structure. The enthalpy of the monoclinic structure is set as zero. The lower panel shows the volume change as a function of pressure for the low pressure and high pressure structure. The experimental data is also plotted for comparison.

experimental diffraction patterns above ~35 GPa can be fitted with a combination of the tetragonal and monoclinic phases, suggesting a sluggish phase transition with increase in pressure. The measured and calculated unit cell volumes are shown as functions of pressure in Figure 6 and are in excellent agreement with experiment at low pressures. We note that the experimental volumes after the phase transition are slightly larger than the theoretical values with this behavior likely due to the mixing of the phases commonly encountered in sluggish phase transitions. We also note that the experimentally observed difference (~0.12 Å) between the "a" and "b" lattice parameters is not well reproduced by the theoretical calculations which find a difference of <0.01 Å (Table 1). The combined effects of phase mixing, defects, and magnetic orderings are likely to be responsible for the observed distortion, although further theoretical investigations are required.

The bulk modulus value was obtained by fitting the volume changes for pressures below 30 GPa with the Birch–Murnaghan equation of state for the tetragonal phase as shown in Figure 7. This analysis leads to the value $B_0 = 86(2)$ GPa with pressure derivative $B_0' = 6$. This value agrees well with the bulk modulus value of $B_0 = 85(6)$ GPa obtained in the neutron diffraction experiments.[13] The bulk modulus determined for $YbMn_2Ge_2$ is also comparable to the bulk moduli determined for other YbT_2X_2 compounds and Yb aluminides and chalcogenides reported in the literature.[22−24]

4.3. Magnetic Structure, Density of States—Theoretical Analyses. The Yb valency and magnetic structure of $YbMn_2Ge_2$ at ambient conditions were investigated by calculating the total energy of crystalline $YbMn_2Ge_2$ as a function of volume for several likely options of magnetic structures and Yb valence. The SIC-LSD method was outlined in section 3. In particular, the Yb valence state is modeled by applying self-interaction corrections to either 13 or 14 f-electron states on each Yb ion. The latter describes the divalent state. With 13 self-interaction corrected f-electrons the 14th electron state is either projected out of the active state space to model the pure trivalent state or allowed to hybridize and form bands, simulating an intermediate valence state. The ratios of the lattice parameters as well as the Ge internal coordinates
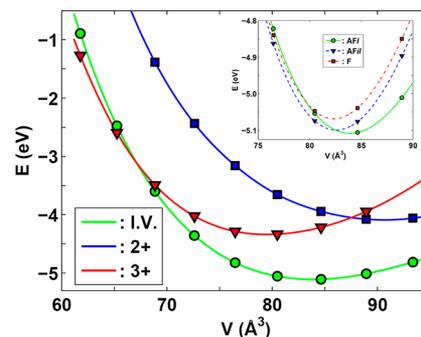
Figure 7. Total energy (in eV per formula unit) versus volume (in Å^3 per formula unit) of $YbMn_2Ge_2$ in the collinear antiferromagnetic phase (AFl) for three different valence scenarios of Yb: circles (I.V., green):, intermediate valence state; squares (blue), divalent Yb ions; triangles (red), trivalent Yb ions. The inset displays the energy of the AFl magnetic structure (circles and full green line), the AFil magnetic structure (triangles and dashed blue line), and the ferromagnetic structure (squares and dashed-dotted red line), in all cases with intermediate valent Yb ions.

were fixed at their experimental values, as determined under ambient conditions, during the variation of the unit cell volume. Figure 7 displays the calculated total energy of $YbMn_2Ge_2$ for these Yb valence scenarios as a function of specific volume assuming the AFl magnetic ordering (i.e., the observed collinear structure in the temperature range $T_{N1} > T > T_{N2}$). As seen from Figure 7, the lowest energy for the AFl structure is found for the intermediate valence state. The effective Yb valence of 2.48 obtained at the equilibrium volume $V_0 = 83.9$ Å^3 is in excellent agreement with the valence $\nu = 2.42$ determined experimentally. As discussed in section 4.1, on compression the calculated effective valence is found to increase rather slowly (see inset of Figure 3), in contrast to the rapid change observed in the experiments. The calculations reveal that the total energy minima for the pure divalent and trivalent states of Yb are higher than the minimum for the intermediate valence state. When volume is decreased from the minimizing value ($V_0 = 83.9$ Å^3), the trivalent and intermediate valence states (circles and triangles in Figure 7) come closer in energy, until at a volume around ~65 Å^3, corresponding to a 23% compression, their enthalpies are equal, and the system will transform into the trivalent state. In contrast, the experimental observation of the transition occurs at just a compression of a few percent. This may be due to overestimation in the present treatment of the bonding associated with the intermediate valence state, where the energy of the "lingering" f-electron essentially is described by the band formation energy as calculated in the local density approximation, which is known to overestimate bonding energies.[39] Another possible cause of the disagreement is that the SIC-LSD theory cannot treat finite temperature for direct comparison with experiments performed at room temperature.

As shown in the inset of Figure 7, the total energy curves of the competing AFil antiferromagnetic structure (i.e., the observed phase at high pressure above 2 GPa, in the nomenclature of ref 18) are very similar to those of the AFl magnetic structure. The total energy of the intermediate valence state of Yb with the AFil magnetic structure is higher by ~8 meV per formula unit compared with the antiferromagnetic AFl structure; this finding agrees well with the observed AFl ground state magnetic structure of $YbMn_2Ge_2$. From the inset to Figure 7, the energy minimum for antiferromagnetic AFil is

seen to occur at slightly lower volume ($\sim$82.5 Å^3) compared with the antiferromagnetic AF*l* structure ($\sim$83.9 Å^3). The SIC-LSD method cannot describe the noncollinear AF*mc* structure—this structure exists below T_{N2} = 185 K and would therefore be appropriate for consideration as a zero temperature theory. For the pure trivalent state, however, the AF*il* magnetic structure is found to exhibit a lower energy minimum than the AF*l* structure by $\sim$60 meV per formula unit, again in agreement with the occurrence of this phase above 2 GPa. The findings summarized in the inset of Figure 7 imply that a magnetic transition from AF*l* to AF*il* should occur at a moderate pressure. The magnetic transition occurs within the Mn layers with intermediate valence Yb ions on both sides of the transition. The transition pressure for this magnetic structural change is calculated to be 1.2 GPa, a number coinciding with the experimental magnetic transition pressure of 1.25 GPa.[13,19,20] However, this agreement is likely to be somewhat fortuitous, since the SIC-LSD theory includes some inaccuracies, for example, with respect to calculated equilibrium volumes.

Furthermore, temperature is not included in the present theory, and as explained above, the observed significant Yb valence change occurring with the magnetic transition is not captured by the theory. We may infer from the calculations, though, that, as a trend, compression will favor the AF*il* magnetic structure with respect to the AF*l* magnetic structure. A structure with ferromagnetic ordering of the Mn moments was also considered. As shown by the inset to Figure 8, the
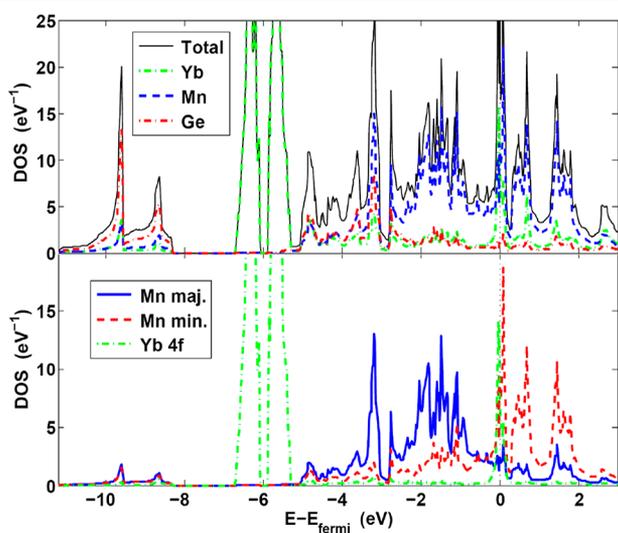
Figure 8. Density of electronic states for YbMn$_2$Ge$_2$ in the coplanar intermediate valence state for experimental lattice parameters at ambient conditions. The upper panel shows the total DOS (thin black line) and partial DOS of Yb (dashed-dotted green), Mn (dashed blue), and Ge (dashed-dotted red). The lower panel shows the spin-decomposed Mn DOS and the Yb 4f-partial DOS. Energy is in eV relative to the Fermi level. The narrow Yb f-peak at the Fermi level reflects the intermediate valence in the SIC-LSD approximation.

energy of this ferromagnetic phase is higher (minimum is 39 meV higher than minimum of AF*l* phase) and remains higher than the energy of the AF*il* phase in the volume range considered. Table 1 summarizes the characteristics of the calculated intermediate valence ground state and compares with available experimental information in addition to structural

details. Several other magnetic states are observed in rare earth compounds of the form RMn$_2$Ge$_2$.[40]

The density of states of YbMn$_2$Ge$_2$ as calculated for the AF*l* state in the intermediate valence scenario is shown in Figure 8 for the experimental crystal structure at ambient conditions. Here, the positions of the localized Yb f-levels were determined by the transition state approximation as discussed in ref 41. The splitting between j = 5/2 and j = 7/2 clearly appears. The Mn d-states dominate the bands in the range from 3 eV below the Fermi level to 2 eV above the Fermi level, however, with a significant degree of hybridization with Ge and Yb states. The Yb 4f-band, which mimics the intermediate valent character, falls at the Fermi level and hybridizes significantly with the Mn states. The width of this band is around 0.15 eV; however, proper account of Coulomb correlation effects would likely lead to narrowing of this band. Upon compression, slight shifts of this Yb 4f-band relative to the dominating Mn minority spin bands at E_f lead to the gradual charge transfer from the Yb band to the Mn bands, which translates into the effective Yb valence change under pressure. The net moment on Mn is 2.09 μ_B.

For comparison we show in Figure 9 the density of states for the same lattice parameters and magnetic structure, however,
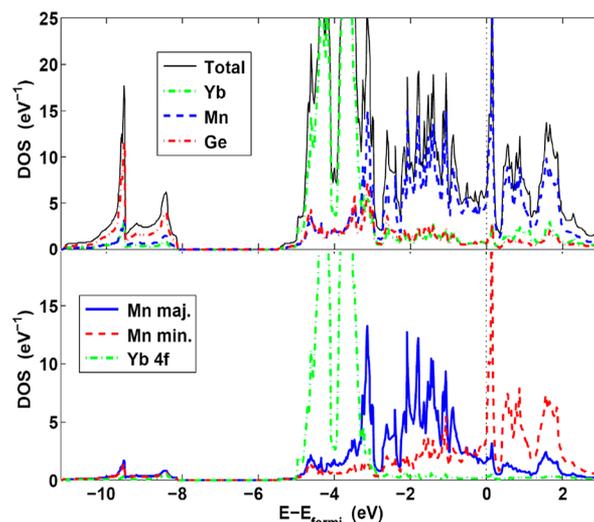
Figure 9. Density of electronic states for YbMn$_2$Ge$_2$ in the planar AF*l* magnetic state with assumed divalent Yb^{2+} ions. Upper panel shows the total DOS (thin black line) and partial DOS of Yb (dotted green), Mn (dashed blue), and Ge (dashed-dotted red). The lower panel shows the spin-decomposed Mn DOS and the Yb 4f-partial DOS. Energy is in eV relative to the Fermi level.

assuming the Yb ions to be divalent. Most distinctly, the narrow f-band around the Fermi level is now absent, having been transferred into the localized f-manifold. The localized f-levels are now situated approximately 2 eV higher compared to the intermediate valence scenario of Figure 8, around 4 eV below the Fermi level as opposed to the position around 6 eV below the Fermi level in Figure 8. This shift is an effect of the increased Coulomb interaction in the f-shell.

5. CONCLUSIONS

The Yb valence and crystal structure of the intermetallic compound YbMn$_2$Ge$_2$ have been measured as functions of pressure up to 40 GPa using RXES and XAS in the PFY mode, together with X-ray diffraction techniques. The Yb effective valence is 2.42(2) at ambient pressure and increases sharply to

2.75 at a pressure of 1.4 GPa. Upon further compression the valence increases more slowly, reaching a nearly trivalent state around 30 GPa. A pressure induced structural phase transition from the tetragonal ($I4/mmm$) structure to a monoclinic ($P1$) phase is observed around 35 GPa. Most distinctly, the new monoclinic phase corresponds to a buckling and rotation of Mn layers. Theoretical calculations were performed with the GGA and SIC-LSD methods. The GGA method was used for a structural search in order to identify the structure of the high pressure phase, which indeed was found to be monoclinic. The SIC-LSD method allows the Yb valence to be investigated under pressure. In agreement with the experimental results an intermediate valence ground state with AF*l* type antiferromagnetic ordering of Mn moments is found. The calculated effective Yb valence is 2.48 at ambient conditions and increases rather slowly with applied pressure in this phase, in contrast to the abrupt increase observed experimentally. This reflects a too large calculated energy separation between competing intermediate valence and trivalent states of the Yb ions.

■ AUTHOR INFORMATION

Corresponding Author

*E-mail: ravhi@physics.unlv.edu.

Notes

The authors declare no competing financial interest.

■ ACKNOWLEDGMENTS

■ REFERENCES

(1) Lawrence, J. M.; Riseborough, P. S.; Park, R. D. *Rep. Prog. Phys.* **1981**, *44*, 3.

(2) Kasuya, T.; Saso, T. *Theory of Heavy Fermions and Valence Fluctuations*; Springer: Berlin,1985.

(3) Hewson, A. C. *The Kondo Problem to Heavy Fermions*; Cambridge University Press: Cambridge, 1993.

(4) Wachter, P. In *Handbook on the Physics and Chemistry of Rare Earths*; Gschneidner, K. A., , Jr., Eyring, L., Lander, G., Choppin, G. R., Eds.; Elsevier: Amsterdam, 1994; Vol. *19*, Ch. 132, p 177.

(5) Svane, A.; Temmerman, W. M.; Szotek, Z.; Petit, L.; Strange, P.; Winter, H. *Phys. Rev. B* **2000**, *62*, 13394.

(6) Parthé, E., Chabot, B. In *Handbook on the Physics and Chemistry of Rare Earths*; Gschneidner, K. A., Jr., Eyring, L., Eds.; Elsevier: Amsterdam, 1984; Vol. *6*, Ch. 48, p 113.

(7) Szytula, A.; Leciejewicz, J. In *Handbook on the Physics and Chemistry of Rare Earths*; Gschneidner, K. A., Jr., Eyring, L., Eds.; Elsevier: Amsterdam, 1989; Vol. *12*, Ch. 83, p 133.

(8) Hofmann, M.; Campbell, S. J.; Edge, A. V. J. *Appl. Phys. A: Mater. Sci. Process.* **2002**, *74* (suppl), S713.

(9) Ryan, D. H.; Cadogan, J. M.; Edge, A. V. J. *J. Phys.: Condens. Matter* **2004**, *16*, 6129.

(10) Szytula, A.; Jezierski, A.; Penc, B.; Hofmann, M.; Campbell, S. J. *J. Alloys Compd.* **2004**, *363*, 46.

(11) Hofmann, M.; Campbell, S. J.; Edge, A.V. J. *J. Magn. Magn. Mater.* **2004**, *272*–*76*, e489.

(12) Hofmann, M.; Campbell, S. J.; Link, P.; Goncharenko, I; Knorr, K. *Physica B* **2004**, *350*, e195.

(13) Hofmann, M.; Campbell, S. J.; Link, P.; Fiddy, S.; Goncharenko, I. *Physica B* **2006**, *385*–*386*, 330.

(14) Jayaraman, A.; Singh, A. K.; Chatterjee, A.; Devi, S. U. *Phys. Rev. B* **1974**, *9*, 2513.

(15) Werner, A.; Hochheimer, H. D.; Jayaraman, A. *Solid State Commun.* **1981**, *38*, 325.

(16) Syassen, K. *Physica B* **1986**, *139/140*, 277.

(17) Hofmann, M.; Campbell, S. J.; Szytula, A. *J. Alloys Compd.* **2000**, *311*, 137.

(18) Venturini, G.; Welter, R.; Ressouche, E.; Malaman, B. *J. Magn. Magn. Mater.* **1995**, *150*, 197.

(19) Fujiwara, T.; Fuji, H.; Uwatoko, Y.; Koyama, K.; Motokawa, M.; Shigeoka, T. *Acta Phys. Pol., B* **2003**, *34*, 1541.

(20) Saiga, Y.; Fujiwara, T.; Kurita, N.; Hedo, M.; Kosaka, M.; Uwatoko, Y. *J. Magn. Magn. Mater.* **2007**, *310*, 1877.

(21) Dallera, C.; Grioni, M.; Shukla, A.; Vanko, G.; Sarrao, J. L.; Rueff, J.-P.; Cox, D. L *Phys. Rev. Lett.* **2002**, *88*, 196403.

(22) Dallera, C.; Annese, E.; Rueff, J.-P.; Palenzona, A.; Vanko, G.; Braicovich, L.; Shukla, A.; Grioni, M. *Phys. Rev. B* **2003**, *68*, 245114.

(23) Kumar, R. S.; Svane, A.; Vaitheeswaran, G.; Kanchana, V.; Bauer, E. D.; Hu, M.; Nicol, M. F.; Cornelius, A. L. *Phys. Rev. B* **2008**, *78*, 075117.

(24) Temmerman, W. M.; Szotek, Z.; Svane, A.; Strange, P.; Winter, H.; Delin, A.; Johansson, B.; Eriksson, O.; Fast, L.; Wills, J. M. *Phys. Rev. Lett.* **1999**, *83*, 3900.

(25) Hammersley, A. P.; Svensson, S. O.; Hanfland, M.; Fitch, A. N.; Hausermann, D. *High Pressure Res.* **1996**, *29*, 301.

(26) Hunter, B. A. *International Union of Crystallography, Commission on Powder Diffraction - Newsletter* **1998**, *20*, 21.

(27) Varma, C. M. *Rev. Mod. Phys.* **1976**, *48*, 219.

(28) Perdew, J. P.; Zunger, A. *Phys. Rev. B* **1981**, *23*, 5048.

(29) Svane, A. *Phys. Rev. B* **1996**, *53*, 4275.

(30) Temmerman, W. M.; Svane, A.; Szotek, Z.; Winter, H.; Beiden, S. Electronic Structure and Physical Properties of Solids: The Uses of the LMTO Method. In *Lecture Notes in Physics*; Dreyssé, H., Ed.; Springer-Verlag: Berlin, 2000; Vol. *535*, pp 286–312.

(31) Strange, P.; Svane, A.; Timmerman, W. M.; Szotek, Z.; Winter, H. *Nature (London)* **1999**, *399*, 756.

(32) Temmerman, W. M.; Petit, L.; Svane, A.; Szotek, Z.; Lüders, M.; Strange, P.; Staunton, J. B.; Hughes, I. D.; Györffy, B. L. In *Handbook on the Physics and Chemistry of Rare Earths*; Gschneidner, K. A., Jr., Bünzli, J.-C. G., Pecharsky, V. K., Eds.; Elsevier: Amsterdam, 2009; Vol. *39*, Ch. 241, p 1.

(33) Svane, A.; Strange, P.; Temmerman, W. M.; Szotek, Z.; Winter, H.; Petit, L. *Phys. Status Solidi B* **2001**, *223*, 105.

(34) Andersen, O. K. *Phys. Rev. B* **1975**, *12*, 3060.

(35) Andersen, O. K.; Jepsen, O. *Phys. Rev. Lett.* **1984**, *53*, 2571.

(36) Oganov, A. R.; Glass, C. W. *J. Phys.: Condens. Matter* **2008**, *20*, 064210.

(37) Perdew, J. P.; Burke, K.; Ernzerhof, M. *Phys. Rev. Lett.* **1996**, *77*, 3865.

(38) http://www.vasp.at/.

(39) Jones, R. O.; Gunnarsson, O. *Rev. Mod. Phys.* **1989**, *61*, 689.

(40) Venturini, G.; Malaman, B.; Ressouche, E. *J. Alloys Compd.* **1996**, *240*, 139.

(41) Svane, A.; Christensen, N. E.; Petit, L.; Szotek, Z.; Temmerman, W. M. *Phys. Rev. B* **2006**, *74*, 165204.